



**HAL**  
open science

## Correcting biases in tropical cyclone intensities in low-resolution datasets using dynamical systems metrics

Davide Faranda, Gabriele Messori, Stella Bourdin, Mathieu Vrac, Soulivanh Thao, Jacopo Riboldi, Sebastien Fromang, Pascal Yiou

### ► To cite this version:

Davide Faranda, Gabriele Messori, Stella Bourdin, Mathieu Vrac, Soulivanh Thao, et al.. Correcting biases in tropical cyclone intensities in low-resolution datasets using dynamical systems metrics. *Climate Dynamics*, 2023, <https://link.springer.com/article/10.1007/s00382-023-06794-8>. 10.1007/s00382-023-06794-8 . hal-03631098v2

**HAL Id: hal-03631098**

**<https://hal.science/hal-03631098v2>**

Submitted on 17 Apr 2023

**HAL** is a multi-disciplinary open access archive for the deposit and dissemination of scientific research documents, whether they are published or not. The documents may come from teaching and research institutions in France or abroad, or from public or private research centers.

L'archive ouverte pluridisciplinaire **HAL**, est destinée au dépôt et à la diffusion de documents scientifiques de niveau recherche, publiés ou non, émanant des établissements d'enseignement et de recherche français ou étrangers, des laboratoires publics ou privés.

1                    Correcting biases in tropical cyclone  
2                    intensities in low-resolution datasets using  
3                    dynamical systems metrics

4                    Davide Faranda<sup>1,2,3\*</sup>, Gabriele Messori<sup>4,5</sup>, Stella  
5                    Bourdin<sup>1</sup>, Mathieu Vrac<sup>1</sup>, Soulivanh Thao<sup>1</sup>, Jacopo  
6                    Riboldi<sup>4</sup>, Sébastien Fromang<sup>1</sup> and Pascal Yiou<sup>1</sup>

7                    <sup>1\*</sup>Laboratoire des Sciences du Climat et de l'Environnement,  
8                    LSCE/IPSL, CEA-CNRS-UVSQ, Université Paris-Saclay,  
9                    Gif-sur-Yvette, 91191, France.

10                    <sup>2</sup>London Mathematical Laboratory, 8 Margravine Gardens  
11                    London, W6 8RH, London, United Kingdom.

12                    <sup>3</sup>LMD/IPSL, Ecole Normale Supérieure, PSL research University,  
13                    Paris, France.

14                    <sup>4</sup>Department of Earth Sciences and Centre of Natural Hazards and  
15                    Disaster Science (CNDS), Uppsala University, Uppsala, Sweden.

16                    <sup>5</sup>Department of Meteorology and Bolin Centre for Climate  
17                    Research, Stockholm University, Stockholm, Sweden.

18                    \*Corresponding author(s). E-mail(s): [davide.faranda@lsce.ipsl.fr](mailto:davide.faranda@lsce.ipsl.fr);

19                    Contributing authors: [gabriele.messori@geo.uu.se](mailto:gabriele.messori@geo.uu.se);

20                    [stella.bourdin@lsce.ipsl.fr](mailto:stella.bourdin@lsce.ipsl.fr); [mathieu.vrac@lsce.ipsl.fr](mailto:mathieu.vrac@lsce.ipsl.fr);

21                    [soulivanh.thao@lsce.ipsl.fr](mailto:soulivanh.thao@lsce.ipsl.fr); [jacopo.riboldi@geo.uu.se](mailto:jacopo.riboldi@geo.uu.se);

22                    [sebastien.fromang@lsce.ipsl.fr](mailto:sebastien.fromang@lsce.ipsl.fr); [pascal.yiou@lsce.ipsl.fr](mailto:pascal.yiou@lsce.ipsl.fr);

23                    **Abstract**

24                    Although the life-cycle of tropical cyclones is relatively well under-  
25                    stood, many of the underlying physical processes occur at scales below  
26                    those resolved by global climate models (GCMs). Projecting future  
27                    changes in tropical cyclone characteristics thus remains challenging. We  
28                    propose a methodology, based on dynamical system metrics, to recon-  
29                    struct the statistics of cyclone intensities in coarse-resolution datasets,  
30                    where maximum wind speed and minimum sea-level pressure may

not be accurately represented. We base our analysis on 411 tropical cyclones occurring between 2010 and 2020, using both ERA5 reanalysis data and observations from the HURDAT2 database, as well as a control simulation of the IPSL-CM6A-ATM-ICO-HR model. With ERA5 data, we compute two dynamical system metrics related to the number of degrees of freedom of the atmospheric flow and to the coupling between different atmospheric variables, namely the local dimension and the co-recurrence ratio. We then use HURDAT2 data to develop a univariate quantile–quantile bias correction conditioned on these two metrics, as well as a multivariate correction method. The conditional approach outperforms a conventional univariate correction of the sea-level pressure data only, pointing to the usefulness of the dynamical systems metrics in this context. We then show that the multivariate approach can be used to recover a realistic distribution of cyclone intensities from comparatively coarse-resolution model data.

**Keywords:** Tropical cyclones, Extreme Event, Bias Correction

## 1 Introduction

Tropical cyclones are among the most devastating natural disasters, often causing fatalities and extensive economic damage (Smith and Katz, 2013; Grinsted et al, 2019). They include several collateral hazards that can have significant impacts on people and property, such as rogue waves, flooding, extreme winds, and tornadoes. The few, most severe episodes account for the bulk of the costs associated with tropical cyclone (Emanuel, 2021). It is thus crucial to model such cyclones correctly. Unfortunately, even state-of-the-art global and regional climate models struggle to reproduce the dynamics of the most severe tropical cyclones (Camargo and Wing, 2016; Roberts et al, 2020b). This is mainly due to their insufficient resolution. Indeed, a grid spacing of the order of 10 kilometers or below is needed (Rotunno et al, 2009; Moon et al, 2020; Murakami et al, 2012; Manganello et al, 2012). Downscaling techniques can be employed to alleviate this issue, but their use is limited by computational costs; furthermore, different downscaling approaches can lead to diverging conclusions (e.g., Caron et al, 2011; Lee et al, 2020; Knutson et al, 2020; Emanuel, 2021). The situation is complicated by the reduced length of records in available tropical cyclone data sets, which mostly rely on satellite data not available before the '80s (Chang and Guo, 2007). This limitation hinders separating significant changes in tropical cyclone properties from decadal variability (Knutson et al, 2019).

Mid-latitude synoptic dynamics mostly originate from the chaotic structure of the motions associated with baroclinic instability (Lorenz, 1990; Schubert and Lucarini, 2015). Tropical cyclones are instead characterized by a rapid organization of unstable flows at the convective scale whose dynamics is turbulent and highly sensitive to boundary conditions (Muller and Romps, 2018;

73 Carstens and Wing, 2020). Here, we investigate whether it may be possi-  
74 ble to exploit this high level of flow organization to obtain reliable statistics  
75 of intense tropical cyclones from relatively coarse-gridded atmospheric data.  
76 To achieve this, we compute two metrics that describe cyclones as states  
77 of a chaotic high-dimensional dynamical system. The first, the local dimension  
78  $d$ , reflects the number of active degrees of freedom of an instantaneous  
79 state of the cyclone. The second, the co-recurrence ratio  $\alpha$ , is a proxy for the  
80 instantaneous coupling between different atmospheric variables which may be  
81 interpreted in the sense of covariability. These metrics have recently provided  
82 insights on a number of geophysical phenomena, including transitions between  
83 transient metastable states (e.g. weather regimes) of the mid-latitude atmo-  
84 sphere (Faranda et al, 2017; Hochman et al, 2021a; Messori et al, 2021), drivers  
85 and predictability of extreme events (Messori et al, 2017; Hochman et al, 2019;  
86 De Luca et al, 2020; Faranda et al, 2020; Hochman et al, 2021b), palaeoclimate  
87 attractors (Brunetti et al, 2019; Messori and Faranda, 2021), slow earthquake  
88 dynamics (Gualandi et al, 2020) and changes in mid-latitude atmospheric pre-  
89 dictability under global warming (Faranda et al, 2019). A benefit over previous  
90 dynamical systems approaches (e.g Wolf et al, 1985; Cao, 1997) is that these  
91 metrics can be easily applied to computationally demanding datasets, such as  
92 climate reanalyses or climate models.

93 Applications of  $d$  and  $\alpha$  in the literature have used an Eulerian approach  
94 over a fixed spatio-temporal domain, rather than tracking the evolution of  
95 specific physical phenomena. Here, we follow the recent work of Faranda et al  
96 (2023) and apply the two metrics in a semi-Lagrangian perspective to char-  
97 acterize the structure of tropical cyclones in the  $d - \alpha$  phase-space. That is,  
98 we compute the metrics on a spatial domain which follows the track of each  
99 cyclone in time. This enables the study of the complex behavior of convectively  
100 unstable flows, by focussing on the evolution of the storm's structure instead  
101 of the storm's motion across a fixed domain (Crisanti et al, 1991; Vulpiani,  
102 2010). The signature of intense cyclones is associated with the presence of  
103 inverse energy cascades as suggested by Levich and Tzvetkov (1985) and, more  
104 recently, by Faranda et al (2018); Dunkerton et al (2009); Tang et al (2015).  
105 Such inverse cascades are associated with potential-kinetic energy conversions  
106 and are particularly notable for intense storms (Bhalachandran et al, 2020).  
107 These energy conversions are related to the deep convection in the eyewall,  
108 that redistributes to the upper troposphere the enthalpy gained thanks to sur-  
109 face heat fluxes in the boundary layer. Such local processes contribute to the  
110 generation of the storms' warm core and, ultimately, to wind intensification  
111 at the larger, sub-synoptic scale of the storm (Emanuel, 1986). We hypothe-  
112 sise that these exchanges have a signature in both the large-scale horizontal  
113 velocity and potential vorticity fields, which are reasonably well-represented in  
114 coarse simulations or reanalyses. If this indeed holds, then the dynamical sys-  
115 tem metrics should be able to distinguish between different storm intensities  
116 due to their different degree of organization and coupling. This would enable  
117 a correction conditioned on  $d$  and  $\alpha$  of cyclone intensity statistics in datasets

118 where we cannot explicitly access the spatial scales underlying the dynamics  
119 of intense tropical cyclones.

120 Bias correction of climate models is a crucial step in improving the accu-  
121 racy of climate predictions, and there is a considerable number of different  
122 bias correction techniques proposed in the literature. For a review of bias cor-  
123 rection methodologies, which is beyond the purpose of this paper, we refer  
124 the reader to [Maraun \(2016\)](#). One widely used method is empirical Quantile  
125 mapping bias correction (QMBC), which has been shown to be effective in  
126 reducing biases in precipitation and temperature data (e.g., [Li et al \(2010\)](#);  
127 [Michelangeli et al \(2009\)](#); [Cannon et al \(2015\)](#); [Cannon \(2018\)](#)). QMBC has  
128 also been applied to assessing the impact of climate change on tropical cyclone  
129 (TC) intensity in medium-resolution global climate models (GCMs) ([Zhao and  
130 Held, 2010](#); [Sugi et al, 2017](#); [Yoshida et al, 2017](#)). These studies have shown  
131 that QMBC is very useful in improving the accuracy of GCM simulations by  
132 matching the distribution of observed data with the model's output. However,  
133 the conventional QMBC has limitations, including not accounting for non-  
134 stationary characteristics of the data. In this study, we propose a new method  
135 for bias correction that implicitly accounts for weak non-stationarity in the  
136 data through the dynamical systems metrics, and that may be easily extended  
137 to explicitly account for non-stationarity by leveraging well-tested approaches.  
138 We demonstrate its effectiveness in improving the accuracy of TC intensity  
139 projections.

140 We base our analysis on best track cyclone data from the HURDAT2  
141 database, which we take as ground truth, ERA5 reanalysis data and a high-  
142 resolution global climate model simulation. We compute the two dynamical  
143 systems metrics using the square root of the kinetic energy  $uv$  [m/s] and the  
144 potential vorticity field  $PV$  [PVU] at the 850 hPa level. The rationale for using  
145  $PV$  follows the works of [Peng et al \(2012\)](#) and [Fu et al \(2012\)](#) who used  $PV$  for  
146 distinguishing developing versus non-developing disturbances. The square root  
147 of the horizontal kinetic energy  $uv$  is relevant to the study of tropical cyclones  
148 because of its direct connection with the wind speed and with the phases of  
149 rapid intensification/decay of the cyclones ([Krishnamurti et al, 2005](#)). The 850  
150 hPa level is chosen because it lies in-between the planetary boundary layer and  
151 the middle troposphere, where most of the potential-kinetic energy conversions  
152 occur in tropical cyclones ([Camargo et al, 2007](#)). Although some of the  
153 information provided by  $PV$  and  $uv$  is redundant, they are analytically con-  
154 nected, and thus we find that their coupling provides nontrivial information  
155 which justifies their use.

156 Our study is organized as follows: first, we describe the data, variables for  
157 cyclone dynamics and the theoretical bases supporting the computation of the  
158 dynamical system metrics. Then, we show the general characteristics of the  
159 phase space of tropical cyclones in reanalysis data for the different variables,  
160 and use these to define a quantile-quantile correction approach for cyclone  
161 intensities conditioned on the two dynamical systems metrics. The correction

162 is performed on ERA5 reanalysis, using sea-level pressure (SLP) from HUR-  
 163 DAT2 as ground truth. We then conduct an out-of-sample test comparing this  
 164 approach to an unconditional quantile–quantile correction. Finally, we test this  
 165 correction on data from a GCM.

## 166 2 Data

### 167 2.1 HURDAT2 tropical cyclone data

168 We follow 197 North Atlantic and 214 eastern North Pacific tropical cyclones  
 169 that occurred between 2010 and 2020, using the HURDAT2 Best Track  
 170 Data (Landsea and Franklin, 2013). We use six-hourly information on the loca-  
 171 tion and central pressure of the cyclones, as well as their time of landfall or  
 172 special intensity report points.

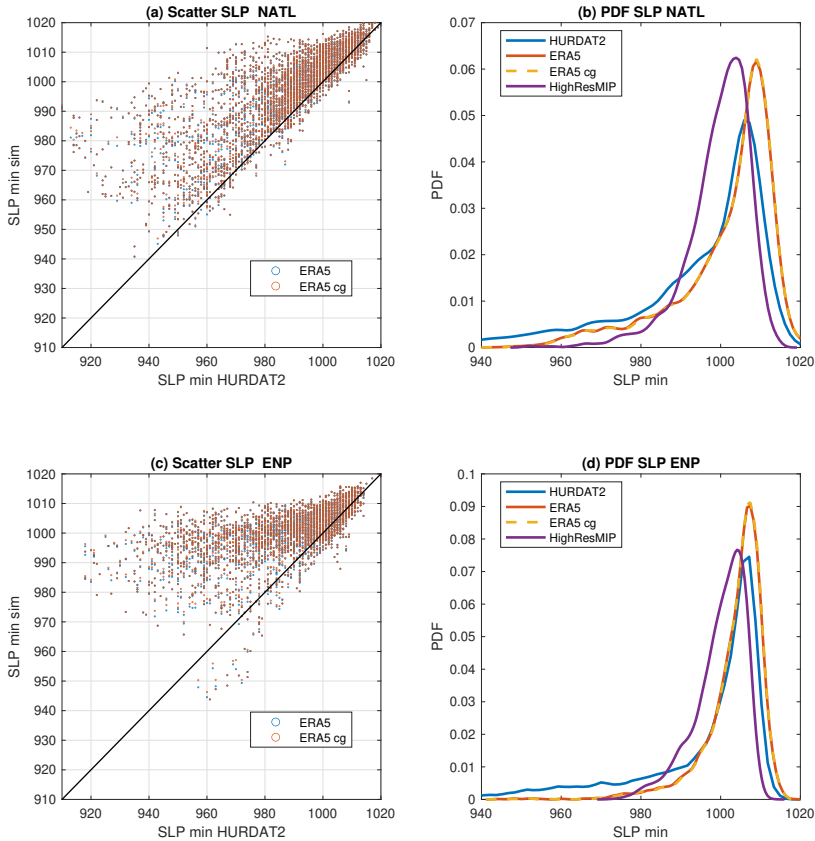
### 173 2.2 Representation of tropical cyclones in ERA5 data

174 We base our analysis on instantaneous<sup>1</sup>  $uv = u^2 + v^2$ ,  $SLP$  and  $PV$  at 850hPa  
 175 from the ERA5 reanalysis (Hersbach et al, 2020), sampled every 6h and addi-  
 176 tionally whenever the HURDAT2 database displays a cyclone landfall entry  
 177 or special intensity report points. The horizontal resolution of the data is  
 178  $0.25^\circ$ . We also make use of ERA5 data coarse-gridded to a  $0.5^\circ$  horizontal  
 179 resolution using a nearest neighbour approach. In the vast majority of cases,  
 180 the SLP difference in the four ERA5 gridpoints around the cyclone core is 1  
 181 hPa or less. Using a nearest neighbour approach thus provides similar results  
 182 to other coarse-graining approaches. The coarse-grained dataset will be here-  
 183 inafter referred to as ERA5 cg, and will be used to evaluate the sensitivity  
 184 of our conclusions to the resolution of the dataset. When comparing ERA5  
 185 to HURDAT2, we verify that the SLP minimum in ERA5 is located within a  
 186 region of  $5^\circ$  of the HURDAT2 cyclone position. For our analysis we do not use  
 187 the wind data because this quantity is often used in different ways (e.g. sus-  
 188 tained winds vs. wind-gusts and with different averaging times) to assess TC  
 189 intensity in reanalyses, models and the HURDAT2 database, while the use of  
 190 minimum SLP is coherent across all datasets.

191 There is often a large discrepancy between the minimum SLP reported  
 192 in HURDAT2 and that in ERA5 (Fig. 1a,c). Especially for the most intense  
 193 cyclones, ERA5 systematically underestimates minimum SLP. The biases are  
 194 larger in the eastern North Pacific than in the North Atlantic basin (cf. Fig. 1a  
 195 and 1c). This affects the capability of ERA5 to accurately assign each tropical  
 196 cyclone to the appropriate Saffir-Simpson category (Simpson and Saffir, 1974),  
 197 which we here use relative to SLP (see Table 1). Indeed, recent research argues  
 198 that SLP is more closely related to cyclone damage than maximum sustained  
 199 winds (Klotzbach et al, 2020). In particular, ERA5 has a negative bias in the  
 200 number of tropical cyclones stronger than category 2, namely  $\min(SLP) < 980$   
 201 hPa. While this bias is present in both the North Atlantic and eastern North

---

<sup>1</sup>We follow here ECMWF’s terminology, see: <https://confluence.ecmwf.int>

6 *Correcting biases in tropical cyclone intensities in low-resolution datasets using dynamical*

**Fig. 1** Scatterplot of minimum SLP for (a) North Atlantic [NATL] and (c) eastern North Pacific [ENP] tropical cyclones in HURDAT2 versus ERA5 and ERA5 cg. Probability density functions of minimum SLP for (b) North Atlantic and (d) eastern North Pacific tropical cyclones in HURDAT2, ERA5, ERA5 cg and the IPSL-CM6A-ATM-ICO-HR model.

202 Pacific basins, in the latter the biases for the most intense cyclones appear  
 203 more severe. This might be due to the more intermittent aircraft reconnais-  
 204 sance activity in that basin with respect to the North Atlantic (Knaff et al,  
 205 2021). The coarse-graining operation does not notably affect the distribution of  
 206 cyclone SLP minima (Fig. 1b, d), likely because of the above-mentioned weak  
 207 SLP variations in the ERA5 dataset in the gridboxes immediately surrounding  
 208 the cyclone core. We underline that the two ERA5 horizontal resolutions used  
 209 here are of the same order of magnitude as those of the HighResMIP (High  
 210 Resolution Model Intercomparison Project, Haarsma et al, 2016) and PRI-  
 211 MAVERA models, which are amongst the current best tools to study climate  
 212 change impacts on tropical cyclones (Roberts et al, 2020a).

## 2.3 Representation of tropical cyclones in IPSL-CM6A-ATM-ICO-HR model data

For the purpose of this study, we used a simulation performed with the IPSL-CM6A model (Boucher et al, 2020). Model configuration is atmosphere-only (ATM) with forced sea-surface temperatures (SST). The physics component of the model is LMDZ6A, as described in Hourdin et al (2020). The dynamical core is Dynamico (Dubos et al, 2015, ICO,), which uses an icosahedral grid. A run at high-resolution (HR) is used, corresponding to  $0.5^\circ$  horizontal resolution. The CM6A version of the IPSL model has 79 vertical levels. The configuration is named IPSL-CM6A-ATM-ICO-HR. The run was performed for the HighResMIP, therefore following the protocol described in (Haarsma et al, 2016). It is a historical run, over the 1950-2014 period (65 years). Greenhouse gases, aerosols and SSTs are forced to the observed values.

We use the TC tracking algorithm from Ullrich et al (2021). We additionally remove tracks starting at latitudes above  $30^\circ$  to minimise incorrect classification of extratropical lows as tropical systems.

The model produces a total of 327 tropical cyclones in the North Atlantic and 989 in the eastern North Pacific (defined following Knutson et al, 2020). Among them, 150 are randomly sampled for each basin, which is deemed a sufficiently large statistical sample for our analysis. The total number of cyclones reproduced by the IPSL-CM6A-ATM-ICO-HR model is in line with that of other HighResMIP models with similar resolution (cf. Roberts et al, 2020b).

A comparison of the distribution of HURDAT2 SLPs with those in the model and in the ERA5 and ERA5 cg data (Fig. 1b, d), suggests that current state-of-the-art GCMs and ERA5 both encounter difficulties when it comes to representing the intensity of tropical cyclones (Kim et al, 2018). Specifically, all three datasets have a sparsely populated left tail of the minimum SLP distribution and, especially for the North Atlantic basin, a different mode when compared to HURDAT2.

## 3 A dynamical systems view of tropical cyclones

In our analysis, for every cyclone we adopt 6-hourly domains of approximately  $1200 \text{ km} \times 1200 \text{ km}$  at latitudes  $10^\circ \text{N} - 25^\circ \text{N}$  ( $41 \times 41$  grid points in ERA5 corresponding to  $10^\circ$  latitude  $\times 10^\circ$  longitude), centred at every timestep on the HURDAT2 cyclone location for ERA5 and centered on the minimum of sea-level pressure for the model simulation. We then consider  $PV$  and  $uv$  at 850 hPa in this domain. Each instantaneous state of the cyclone, as represented by these variables and domains, corresponds to a point along a phase-space trajectory representing the cyclone's evolution. We sample this trajectory at discrete intervals determined by the temporal resolution of our data. Our aim is to diagnose the dynamical properties of the instantaneous (in time) and local (in phase-space) states of the cyclone (physical space in Fig. 2). To do so, we leverage two metrics issuing from the combination of extreme value theory with Poincaré recurrences (Freitas et al, 2010; Lucarini et al, 2012,



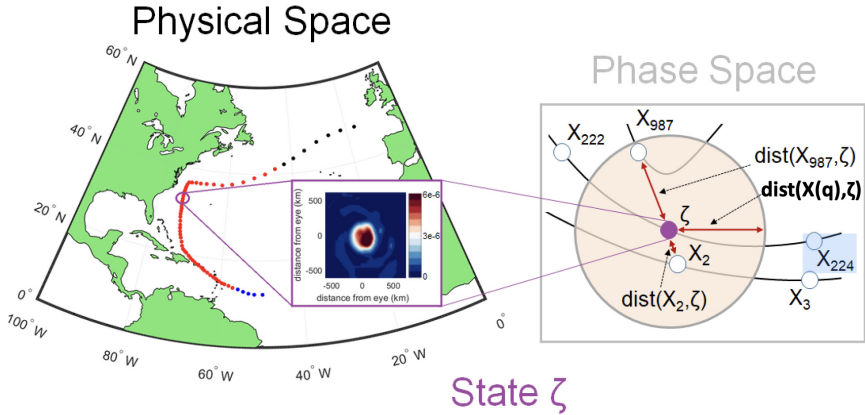


**Fig. 2** Schematic of the computation of the dynamical systems metrics for an instantaneous state of a tropical cyclone. We take a snapshot of the cyclone in physical space (black quadrant), PV in this example, which corresponds to state  $\zeta$  in our phase space. The shaded circle is a 2D representation of the surface determined by the high threshold  $s(q, \zeta)$ , which defines recurrences of  $\zeta$ . The distances between measurements defined by  $\text{dist}(X_i, \zeta)$  are marked by double-headed arrows. For all points within the hyper-sphere,  $\text{dist}(X_i, \zeta) < s(q, \zeta)$  and  $g(X_i, \zeta) > s(q, \zeta)$  hold. Here,  $i$  represents the timestep in the dataset. In the schematic, only two measurements qualify as recurrences: timesteps 2 and 987 (adapted from [Messori and Faranda \(2021\)](#)).

256 [2016](#)). Recurrences are temporally separated  $PV$  or  $uv$  states that resemble  
 257 each other. As we discuss below, identifying these recurrences is instrumental  
 258 to compute the two dynamical systems metrics.

259 We first calculate TC-centered maps of  $PV$  and  $uv$  to define the TC state  
 260  $i$ , where  $i = 0, 1, \dots, T - 1, T$  represents a given timestep in our dataset,  $T$   
 261 being the total number of timesteps. We then normalize each distance by their  
 262 respective norms, which yields  $PV_i$  and  $uv_i$ , respectively. Finally, we define  
 263 the TC state at a given timestep,  $X_i$ , as the pair of  $PV_i$  and  $uv_i$  maps at  
 264 that timestep. We thus construct a semi-Lagrangian framework tracking each  
 265 cyclone. We take each pair of maps  $X_i$  in turn as the reference state  $\zeta$  in our  
 266 calculation (phase space in Fig. 2). We then define logarithmic returns as:

$$g(X_i, \zeta) = -\log[\text{dist}(X_i, \zeta)] \quad (1)$$

267 Here, we define  $\text{dist}$  as the Euclidean distance between pairs of maps, but  
 268 it can be chosen as any distance metric between two vectors. In principle,  $\zeta$   
 269 can be any state (and does not have to belong in the available  $X_i$ ). In prac-  
 270 tice,  $\zeta$  is one of the  $X_i$ , and the  $\log \text{dist}$  is computed for all other time steps,  
 271 as  $\log(\text{dist}(X, X))$  is not defined. Note that the distances between maps are  
 272 computed by respecting the order of the grid points but without specifying  
 273 their actual position on the maps (longitude and/or latitude). The logarithmic  
 274 weight comes directly from the Poincaré recurrence theorem, which states  
 275 that the probability of hitting a ball centered on a state in phase space gets  
 276 exponentially small when linearly reducing the radius of the ball. Since  $\text{dist}$

277 tends to zero as pairs of  $X_i$ s increasingly resemble each other, the series of log-  
 278 arithmic returns  $g_i$  takes large values for  $X_i$  closely resembling  $\zeta$ . The minus  
 279 sign in Eq. 1 has the function to convert the minima of the distances into  
 280 the maxima of  $g$ , as it is common practice in extreme value theory to define  
 281 extreme value distributions for maxima rather than for minima. In Fig. 2,  
 282 an example of the phase space and the geometrical object defined above is  
 283 provided: the shaded circle is a 2D representation of the surface (in general  
 284 this is a hyper-sphere for higher dimension) determined by the high thresh-  
 285 old  $s(q, \zeta) = g(X(q), \zeta)$ , which defines recurrences of  $\zeta$ . The distances between  
 286 measurements are marked by double-headed arrows. For all points within the  
 287 hyper-sphere,  $\text{dist}(X_i, \zeta) < \text{dist}(X(q), \zeta)$  and  $g(X_i, \zeta) > s(q, \zeta)$  hold.

288 We next define exceedances as  $u(g, \zeta) = \Pr(g | g(X_i, \zeta) > s(q, \zeta))$ , where  
 289  $s(q, \zeta)$  is a high threshold corresponding to the quantile  $q$  of  $g(X_i, \zeta)$ . These are  
 290 effectively the previously-mentioned Poincaré recurrences, for the chosen state  
 291  $\zeta$  (phase space in Fig. 2). The Freitas-Freitas-Todd theorem (Freitas et al, 2010;  
 292 Lucarini et al, 2012) states that the cumulative probability distribution  $u(\zeta) =$   
 293  $F(g, \zeta)$  can be approximated by the exponential member of the Generalised  
 294 Pareto Distribution (i.e. with shape and location parameters equal to zero).  
 295 We thus have that:

$$u(g, \zeta) = F(g, \zeta) \simeq \exp \left[ -\frac{g(\zeta)}{\sigma(\zeta)} \right] \quad (2)$$

296 The parameters  $u$  and  $\sigma$ , the scale parameter of the Generalized Pareto  
 297 Distribution, depend on the chosen state  $\zeta$ . From the above, we can define  
 298 the local dimension  $d$  as:  $d(\zeta) = 1/\sigma(\zeta)$ , with  $0 < d < +\infty$ . The Freitas-  
 299 Freitas-Todd theorem thus enables us to estimate numerically  $d$  from a series  
 300 of  $uv$  or  $PV$  data over the semi-Lagrangian domain based on their Poincaré  
 301 recurrences. The numerical procedure is rather simple: i) we fix  $\zeta = X_i$  for a  
 302 given time step  $i$ , ii) we fix  $s$  to be the threshold corresponding to the quantile  
 303  $q = 0.98$ . iii) we obtain all the  $u(\zeta)$ , namely the 2% (because  $q = 0.98$ ) of maps  
 304 having the smallest euclidean distances from  $\zeta$ , iv) we use the fact that Eq.2  
 305 is an exponential to estimate  $\sigma$ , its standard deviation, as the average value of  
 306  $u$  once we subtract  $s$ . Here we are just using the fact that in the exponential  
 307 function, average and standard deviation are equal.

308 Next, we introduce logarithmic returns and high thresholds separately for  
 309  $PV$  and  $uv$  as  $g(PV_i)$ ,  $s_{PV}(q)$  and  $g(uv_i)$ ,  $s_{uv}(q)$  respectively. These allow us to  
 310 investigate the way in which  $PV$  and  $uv$  co-vary by defining the co-recurrence  
 311 ratio  $\alpha$ :

$$\alpha(\zeta) = \frac{\nu[g(PV_i) > s_{PV}(q) | g(uv_i) > s_{uv}(q)]}{\nu[g(PV_i) > s_{PV}(q)]} \quad (3)$$

312 with  $0 \leq \alpha \leq 1$ . Here,  $\nu[-]$  is the number of events satisfying condition  $[-]$ ,  
 313 and all other variables are defined as before. In practice, if all  $PV$  recurrences  
 314 match a  $uv$  recurrence, then the number of conditional  $PV$  events (numerator)  
 315 is the same as the number of unconditional  $PV$  events (denominator) and  
 316 hence  $\alpha = 1$ . In contrast, if  $PV$  recurrences never match  $uv$  recurrences, then

the numerator is zero and hence  $\alpha = 0$ . By definition,  $\alpha$  is symmetric with respect to the choice of variable ( $PV$  or  $uv$ ), since  $\nu[g(PV_i) > s_{PV}(q)] \equiv \nu[g(uv_i) > s_{uv}(q)]$ . In other words, the number of events above a given quantile is the same for either variable, given that they are both taken from the same set of TC snapshots. The section "Code availability" provides information on how to download the package used to compute  $d$  and  $\alpha$ .

While the derivation of  $d$  and  $\alpha$  may seem very abstract, the two metrics can be related intuitively to the physical properties of the tropical cyclones.  $d$  is a proxy for the active number of degrees of freedom of the cyclones' instantaneous states, while  $\alpha$  measures the coupling between different variables. The relationship between dynamical systems metrics and the structure of tropical cyclones is elucidated in Figure 3.  $d$  and  $\alpha$  are anti-correlated: low dimensionality is generally associated to a high coupling between the  $PV$  and  $uv$  maps, while the opposite holds for high dimensionality (Fig. 3a). Most of the considered time steps fall in a regime of relatively low dimensionality relative to the number of gridpoints in the lagrangian domain ( $41^2$ ), and of low coupling. We first investigate the  $uv$  and  $PV$  atmospheric patterns corresponding to these timesteps. To do so, we consider all points below the 0.95 quantiles of the  $d$  and  $\alpha$  distributions, corresponding to thresholds of  $d_H=30$  and  $\alpha_H=0.35$ . These data show a clear, albeit relatively weak, cyclonic structure in  $PV$ , with values peaking at  $\sim 2$  PVU (Fig. 3b). The  $uv$  pattern also reflects a cyclonic structure, with values peaking at  $\sim 12$  m s<sup>-1</sup> (Fig. 3e). The picture is radically different for cyclone timesteps with  $d > d_H$  or  $\alpha > \alpha_H$  (Fig. 3c,d,f,g). High values of  $d$  feature a smaller, weaker  $PV$  core than the bulk of the data, which is reflected in low values of the square root of the kinetic energy (Fig. 3c,f). High values of  $\alpha$  instead correspond to an intense cyclonic  $PV$  core and a correspondingly high  $uv$  around it (Figs. 3d,g). The same qualitative features emerge also for the ERA5 cg and HighResMIP data (not shown). To illustrate this for single cyclones, Fig. 4 shows an example of two snapshots: one with very high  $\alpha$  and low  $d$  and one with very low  $\alpha$  and high  $d$ . These two examples confirm the conclusion drawn from the composite means, although we cannot directly compare the results presented in Figs. 3-4 because the first is about composite averages while the second about single cases.

These results reflect the high degree of symmetry and organization found in intense tropical cyclones with respect to weaker disturbances (e.g., Emanuel, 1986, 1997; Montgomery and Smith, 2017). Intense tropical cyclones display a quasi-axisymmetric shape: a state where very few degrees of freedom (i.e., low  $d$  values, which typically correspond to high  $\alpha$  values) are needed to describe their dynamics because of the air parcels all aligning with the cyclones' circulation. On the contrary, the cyclones with higher dimensionality likely display asymmetric or multiple  $PV$  patches (as for the example shown in Fig. 4b), with a less organised kinetic energy landscape. This variable geometry of the  $PV$  pattern may explain the different degrees of coupling between  $uv$  and  $PV$ .

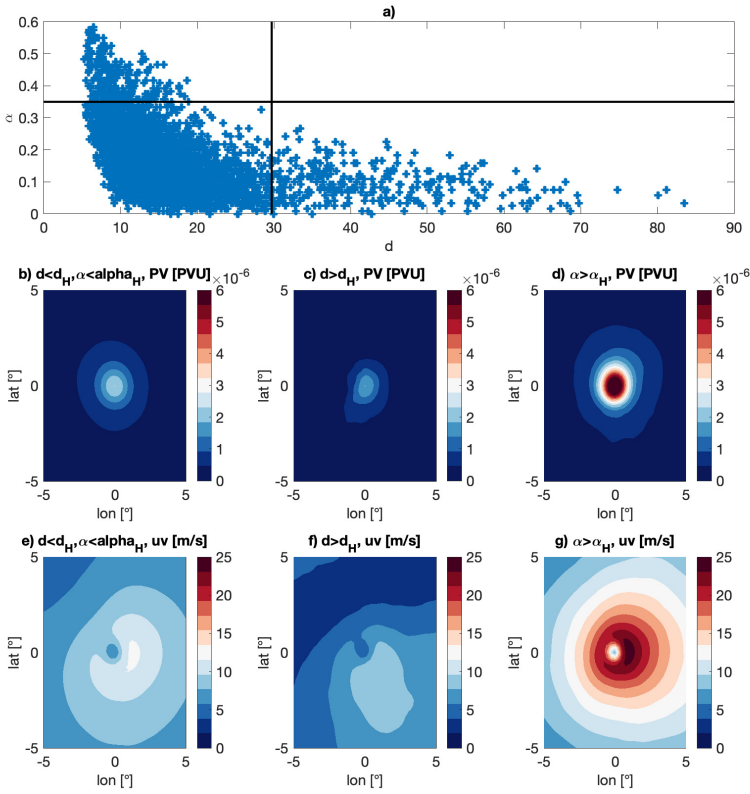


**Fig. 3** The scatter plot displays the values of the local dimension  $d$  and the co-recurrence  $\alpha$  computed on ERA5  $uv$  and  $PV$  maps during tropical cyclone timesteps in the NATL basin. The vertical and horizontal black solid lines mark the 0.95 quantiles of the  $d$  and  $\alpha$  distributions, namely  $d_H$  and  $\alpha_H$ , respectively. The maps show composites of  $PV$  (b–d) and  $uv$  (e–g) for  $d < d_H, \alpha < \alpha_H$  (b,e),  $d > d_H$  (c,f) and  $\alpha > \alpha_H$  (d,g).

362 The connection between  $d$ ,  $\alpha$  and cyclone intensity broadly holds when  
 363 diagnosing the intensity of the cyclones using the minimum SLP, computed  
 364 from gridded data (Fig. 5). In general, large values of  $\alpha$  (colorscale) correspond  
 365 to low values of the minimum SLP in both the North Atlantic and eastern  
 366 North Pacific basins. Moreover, the most intense tropical cyclones phases are  
 367 marked by a low dimension  $d$ . Similar conclusions hold for the HighResMIP  
 368 data, as further discussed in Sect. 4b. Remarkably, the coarse-graining operation  
 369 on ERA5 data does not alter sensibly the dynamical properties  $d$  and  
 370  $\alpha$ , and the two metrics maintain roughly the same range of values as in the  
 371 original  $0.25^\circ$  reanalysis (Fig. 5b, d). The explanation for this stability follows  
 372 that given in Faranda et al (2017) for the SLP data over the North Atlantic:

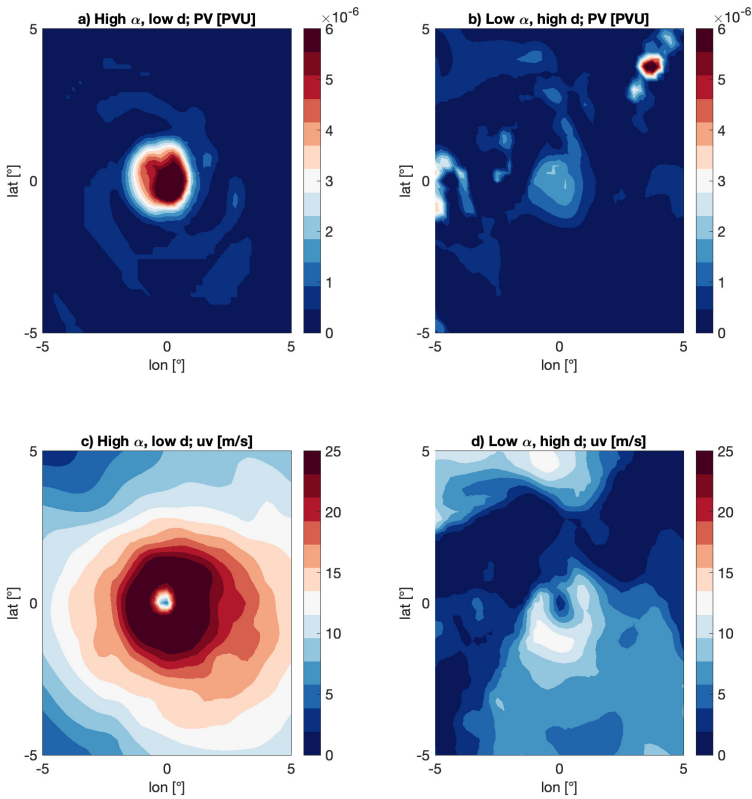


**Fig. 4** As Fig. 3b–g, but for an example of a single cyclone snapshot with  $\alpha = 0.61$  and  $d = 6.02$  (a,c) and  $\alpha = 0.08$  and  $d = 12.36$  (b,d).

373 the dynamical systems metrics are practically insensitive to resolution, pro-  
 374 vided that the resolution is sufficient to represent the underlying dynamics of  
 375 the data. This is the case here since, as previously discussed, ERA5 cg and  
 376 ERA5 share near-identical distributions of cyclone SLP minima.

377

## 378 4 Bias Corrections of tropical cyclone sea-level 379 pressure minima

### 380 4.1 Bias Corrections of ERA5 tropical cyclone sea-level 381 pressure minima

382 We perform two bias corrections for ERA5 minimum sea-level pressure. In  
 383 both cases we prepare our data as follows. Firstly, we rearrange our set of

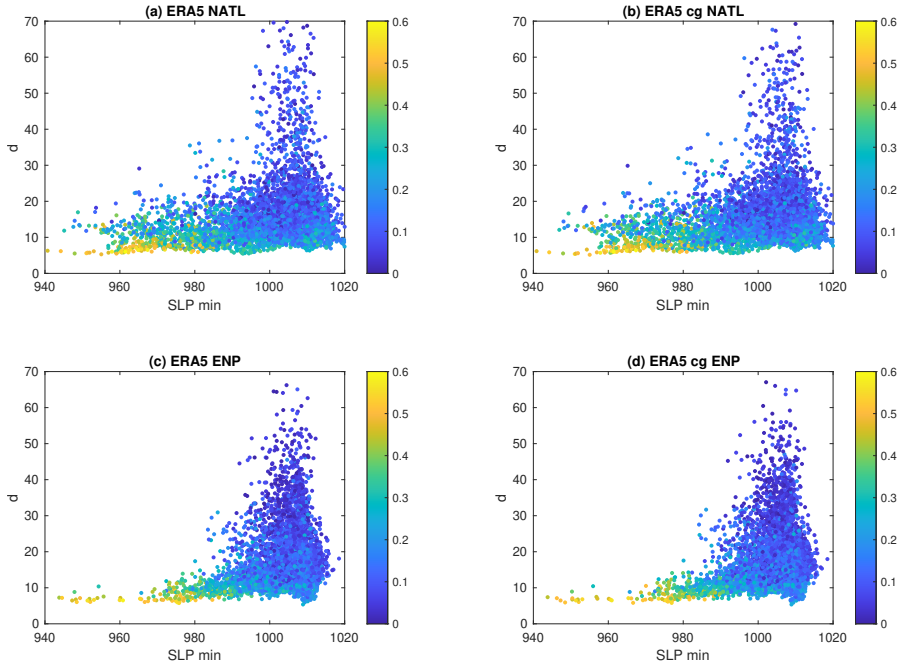


**Fig. 5** Scatterplots of minimum SLP vs local dimension  $d$  and co-recurrence ratio  $\alpha$  (colorscale) calculated on  $uv$  and  $PV$  at 850 hPa for (a,c) ERA5 and (b,d) ERA5 cg, in the (a,b) North Atlantic [NATL] and (c,d) eastern North Pacific [ENP] basins.

384 tropical cyclones randomly. This mixes tropical cyclones from different years  
 385 and different parts of the cyclone season in the training and in the verification  
 386 datasets. We thus avoid intraseasonal effects and possible non-stationarities  
 387 linked to anthropogenic climate change or interannual variability of the  
 388 atmospheric circulation. We then consider the first 4000 datapoints of our  
 389 rearranged HURDAT2 SLP minima for each basin as training data and the  
 390 remaining 2029 datapoints for the North Atlantic basin and 2313 datapoints  
 391 for the eastern North Pacific basin as verification data. This same split is also  
 392 applied to ERA5 cg.

393

394 We next define objective metrics to determine whether our bias corrections  
 395 improve the cyclone intensities. We use the original [Simpson and Saffir](#)  
 396 (1974) scale of tropical cyclones classification based on the SLP minima and  
 397 define cyclone categories for the verification datasets (Table 1). We define two  
 398 error metrics: the total count of tropical cyclones time-steps with the wrong  
 399 category  $Err_T$ , and the count of major tropical cyclones (intensity  $\geq 3$ ) with  
 400 wrong category  $Err_C$ .

401

402 The first bias correction we implement is an unconditional quantile-  
 403 quantile correction. We begin by subtracting the median of the distributions  
 404 of SLP minima from the data, which we then add back at the end of the

405 procedure. We then compute the difference  $\Delta q$  between the empirical cumu-  
 406 lative density functions (ECDFs) of SLP minima in HURDAT2 with respect  
 407 to ERA5 and ERA5 cg evaluated at 100 quantile values  $q$ . For each data  
 408 to correct, the closest quantile  $q^*$  in the ECDF(ERA5) or ECDF(ERA5 cg)  
 409 dataset is found and the value  $\Delta q^*$  is added to the original value.

410 The second bias correction approach is conditioned on the dynamical sys-  
 tems metrics. The results presented in Figures 3 and 5 show that we can  
 discriminate intense tropical cyclones as those having a large value of  $\alpha$  and a  
 small value of  $d$ . We test several  $d_H$  and  $\alpha_H$  pairs (using the same convention  
 of Fig.3) to separate the training dataset into intense ( $d < d_H$ ,  $\alpha > \alpha_H$ ) and  
 non-intense cyclones. We next apply the previously described quantile-quantile  
 correction to the two subsets of cyclones separately. We then use a grid-search  
 approach and scan all combinations of  $10 \leq d \leq 38$  and  $0.1 \leq \alpha \leq 0.34$ , with  
 resolution  $\Delta d = 1$  and  $\Delta \alpha = 0.1$ , to find the values  $d_c$  and  $\alpha_c$  that minimise  
 the total error

$$Err = Err_T(ATL) + Err_T(ENP) + Err_C(ATL) + Err_C(ENP). \quad (4)$$

411 We additionally impose that the chosen values improve upon the unconditional  
 412 correction for both basins and both  $Err_T$  and  $Err_C$ . By randomizing cyclone  
 413 timesteps, we obtain two different sets of 100 realizations for ERA5 and ERA5  
 414 cg training datasets, respectively, which allow to compute two distributions  
 415 each containing 100 values of  $d_c$  and  $\alpha_c$ . The boxplots of such distributions are  
 416 presented in Fig.6. We then select the median over each sample. This analysis  
 417 yields  $d_c = 21$  and  $\alpha_c = 0.16$  for ERA5 and  $d_c = 19$ ,  $\alpha_c = 0.165$  for ERA5  
 418 cg. The standard deviations of  $d_c$  and  $\alpha_c$  are respectively 4 and 0.04. We can  
 419 deduce that the minimisation has some sensitivity to the choice of samples. We  
 420 will refer to these parameters as the best set that realizes the bias correction  
 421 for the data presented in this study.

422 We illustrate in detail the improvement obtained with the two bias correc-  
 423 tion approaches in Figures 7-8. Panels (a,b) show that the ECDFs of bias-  
 424 corrected SLPs are closer to the verification dataset HURDAT2 than the non-  
 425 corrected ones. However, panels (c,d) show that the correspondence of observed  
 426 versus modelled SLPs for individual cyclones is not necessarily improved by  
 427 the bias correction. Specifically, for some of the tropical cyclone timesteps,  
 428 the bias correction attributes a higher category than the original data. This  
 429 is shown in panels (e,f) in terms of  $\Delta$  between the categories as estimated for  
 430 ERA5 (cg) data relative to HURDAT2. Finally panels (g,h) show the evident  
 431 improvements in terms of intensity histograms: the original non corrected data  
 432 virtually have no category 4 or 5 tropical cyclones, whereas with the correc-  
 433 tions we are able to retrieve the full cyclone intensity spectrum. The difference  
 434 between ERA5 and ERA5 cg is limited, although a comparison of panels (d,h)  
 435 between Figs. 7 and 8 evidences that the coarse-graining does have some effect  
 436 on the most intense cyclones. As previously noted, a clear difference emerges  
 437 between the NATL and ENP basins, with the latter generally showing larger

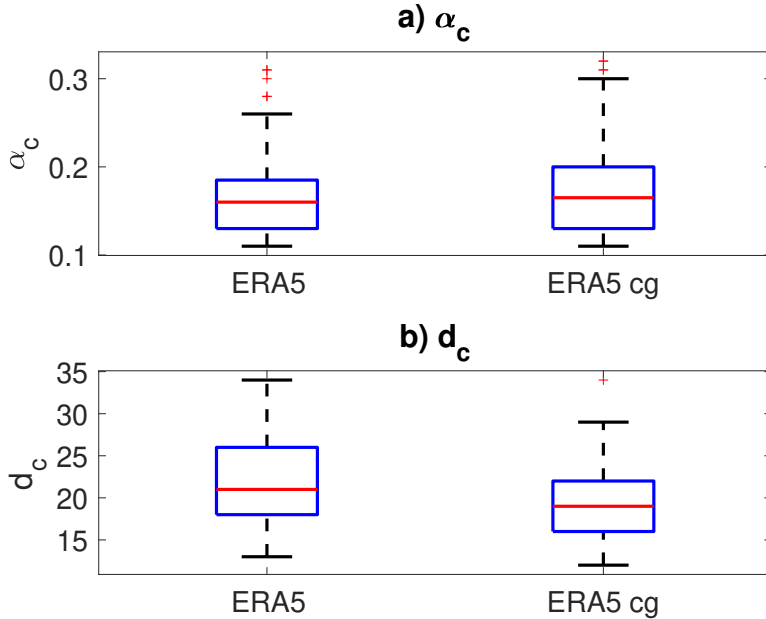


**Fig. 6** Boxplots for 100 realizations of the grid search procedure used to estimate the values of  $\alpha_c$  and  $d_c$  which minimize the total error in Eq. 4. On each box, the central mark indicates the median, and the bottom and top edges of the box indicate the 25th and 75th percentiles, respectively.

438 biases for both the uncorrected and corrected data. The difference between  
 439 the conditional and unconditional bias corrections also emerges chiefly in the  
 440 ENP. Indeed, the two perform comparably in the NATL, while in ERA5 and  
 441 especially in ERA5 cg, the conditional correction shows a vastly improved  
 442 performance.

Category	wind [m/s]	minimum sea-level pressure [hPa]
1	33–42	$\geq 980$
2	43–49	965–979
3	50–58	945–964
4	59–69	920–944
5	>69	$\leq 920$

**Table 1** Saffir-Simpson tropical cyclone intensity classification.

## 443 4.2 Bias Corrections of HighResMip tropical cyclone 444 sea-level pressure minima

445 When looking at the cyclone SLP minima for the HighResMIP data, we remark  
 446 immediately the virtual lack of minima below 960 hPa and the reduced range



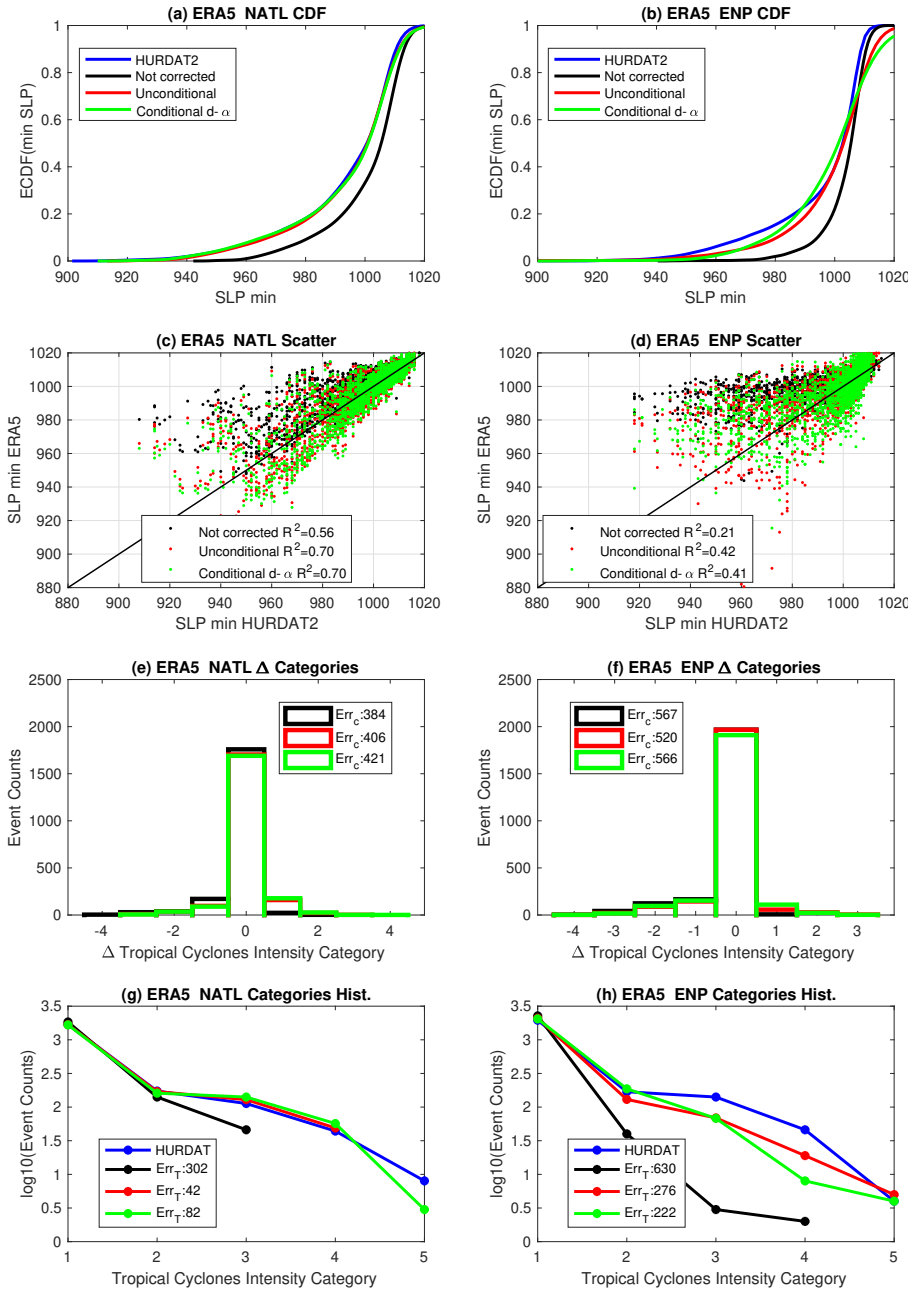


**Fig. 7** Unconditional bias correction and bias correction conditioned on the dynamical systems metrics for the best  $d$  and  $\alpha$  parameters combination (see Fig. 6,  $\alpha_c = 0.16$ ,  $d_c = 21$ ) for a realization of the ERA5 data sample. (a,b) Empirical cumulative density functions (ECDFs), (c,d) scatter plots, (e,f) error  $Err_c$  in category intensities (negative values imply underestimation, positive values overestimation), (g,h) histogram of category intensities and  $ERR_T$  in the inset. (a,c,e,g) North Atlantic [NATL], (b,d,f,h) eastern North Pacific [ENP] basins. See legends for details.

Correcting biases in tropical cyclone intensities in low-resolution datasets using dynamical s

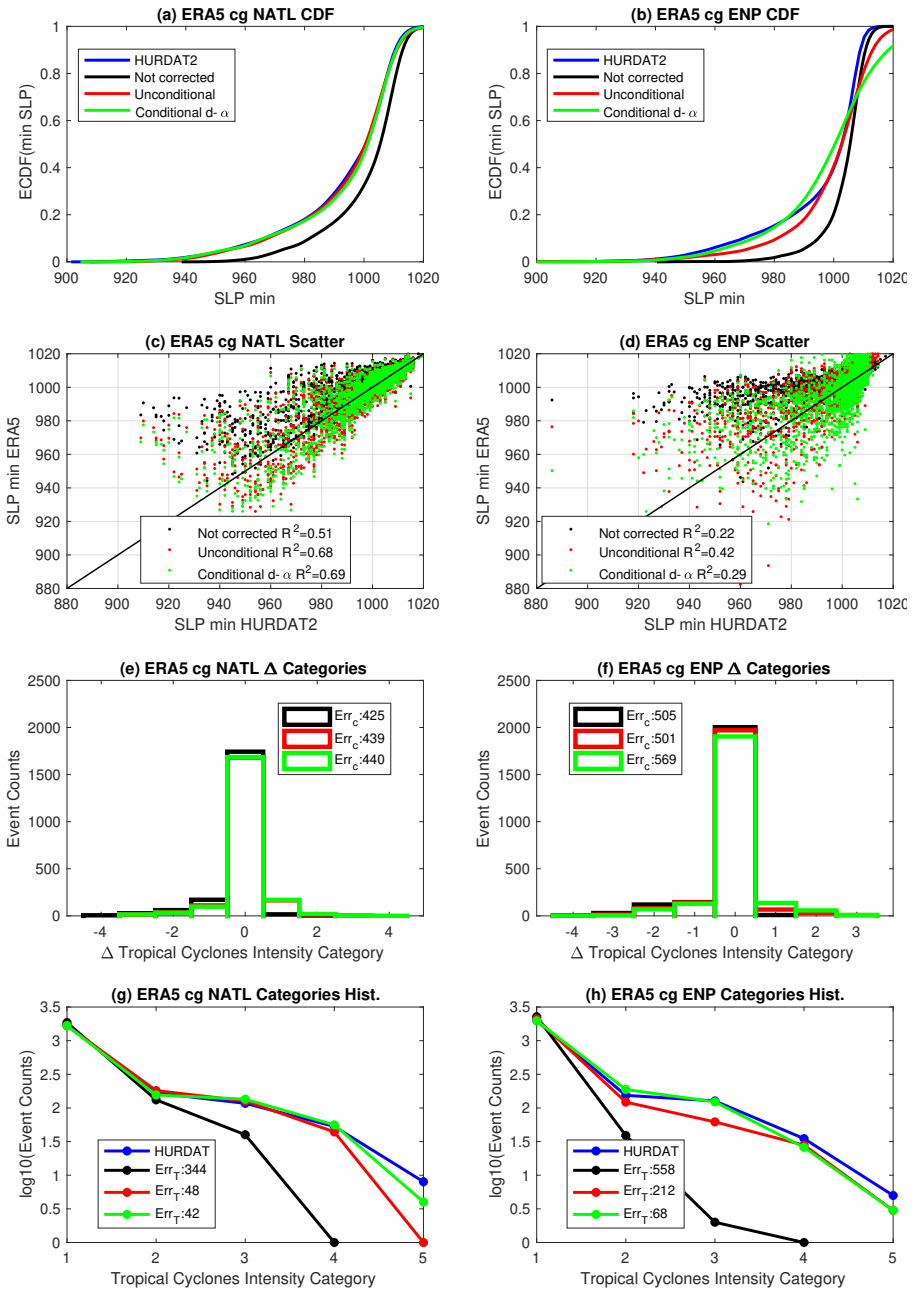


**Fig. 8** As in Fig. 7 but for a realization of the ERA5 cg data sample, using  $\alpha_c = 0.165$ ,  $d_c = 19$ .

of  $d$  and  $\alpha$  values compared to ERA5 or ERA5 cg data (cf. Fig. 9a,c, and 5). These results point to a different dynamical representation of tropical cyclones in HighResMIP. The consequence is that the statistical dependencies between SLP,  $d$  and  $\alpha$  in HighResMIP are not the same as in the reference data (ERA5 and HURDAT). Up to now, the unconditional and conditional bias correction methods applied to adjust cyclone properties were univariate. Hence, dependencies between the three variables (i.e. SLP minima,  $d$  and  $\alpha$ ) were not corrected by the unconditional approach, and only partly with the conditional one. Thus, the resulting tri-variate dependence structures were likely not appropriately represented by the corrected data. To account for this, we now also make use of a multivariate bias correction (MBC) method to adjust not only the univariate distributions but also the dependence between the three variables of interest. To do so, the “Rank Resampling for Distributions and Dependencies” (R2D2) method is applied to adjust jointly (SLP minima,  $d$ ,  $\alpha$ ). R2D2 relies on an analogue-based method applied to the ranks of the time series to be corrected rather than to their “raw” values (Vrac, 2018). This MBC method can be easily designed to adjust both inter-variable, inter-site and temporal properties (Vrac and Thao, 2020) but is used only in its inter-variable configuration in the present study. Figure 9 shows the scatterplots of minimum SLP vs local dimension  $d$  and co-recurrence ratio  $\alpha$  without (a,c) and with (b,d) R2D2 correction. The R2D2 correction retrieves SLP minima of order 920 hPa as well as extends the range of values of  $d$  and  $\alpha$ , reproducing a pattern closer to the one observed in ERA5.

We next apply the unconditional and conditional bias-correction methodologies, as well as the R2D2 method to the HighResMIP simulations. We do not apply the R2D2 method to ERA5 because this is our reference dataset for the computation of the dynamical systems metrics. The main difference in applying the bias correction to model data rather than to reanalysis is that the correction has to be fitted and applied directly to free-running HighResMIP simulations. In such a context, cross-validation techniques for corrections evaluation have been recently heavily criticized (Maraun and Widmann, 2018) due to the influence of the model internal variability on the correction results. Hence, in the following, no separation into training and test data is performed: we correct the bulk cyclone statistics for all selected cyclones in the IPSL-CM6A-ATM-ICO-HR simulation. We first estimate the ECDFs and compute the  $\Delta$  function between HighResMIP and HURDAT2 data. We then correct the full dataset using the unconditional, conditional on  $\alpha$ ,  $d$  – using the ERA5 cg values  $d_c$  and  $\alpha_c$  – and R2D2 corrections. The results are shown in Figure 10. For the ECDFs (panels a,c), corrections obtained with or without the dynamical systems metrics improve, once again, the distribution of SLP minima. The conditional and unconditional corrections appear comparable in the NATL, but show a clear difference in the ENP. The R2D2 correction is virtually indistinguishable from HURDAT in both basins. When looking at the tropical cyclone intensities (panels b,d) we observe that the R2D2 correction of SLP minima provides a distribution of intensities which is very close to

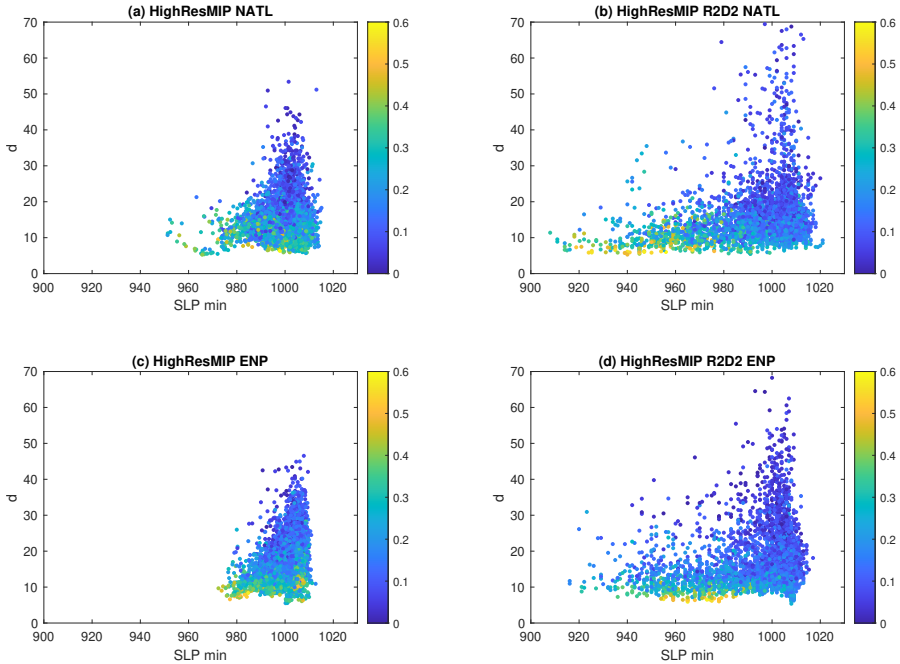


**Fig. 9** Scatterplots of minimum SLP vs local dimension  $d$  and corecurrence ratio  $\alpha$  (color-scale) calculated on  $uv$  and  $PV$  at 850 hPa for (a,c) HighResMIP; (b,d) HighResMIP corrected with R2D2, in the (a,b) North Atlantic [NATL] and (c,d) eastern North Pacific [ENP] basins.

492 that of the HURDAT2 data in both basins. Over the NATL, the R2D2 shows  
 493 a clear improvement over the other corrections. In the ENP, it is close to the  
 494 unconditional correction, which outperforms the conditional correction. Over-  
 495 all, these results suggest that, when applying R2D2, we are able to take into  
 496 full account the information provided by the two dynamical systems metrics.

## 497 5 Summary and implications of the results

498 Starting from the observation that gridded datasets of tropical cyclones have  
 499 a large bias in the representation of the intensity of extreme cyclones, we have  
 500 introduced a bias-correction procedure. We have used: i) an unconditional  
 501 quantile–quantile correction of the sea-level pressure minima of cyclones  
 502 timesteps towards the HURDAT2 reference dataset; ii) a correction condi-  
 503 tioned on two dynamical systems metrics (local dimension and co-recurrence  
 504 ratio); and iii) the R2D2 correction. We have applied the first two approaches  
 505 to ERA5 data, both at the highest available resolution and in a coarse-  
 506 grained version. We have further applied all three approaches to data from  
 507 the IPSL-CM6A-ATM-ICO-HR HighResMIP model. When using the dynamical  
 508 systems metrics, we use the dynamical information from an underlying  
 509 reduced phase space incorporating the square root of the horizontal kinetic

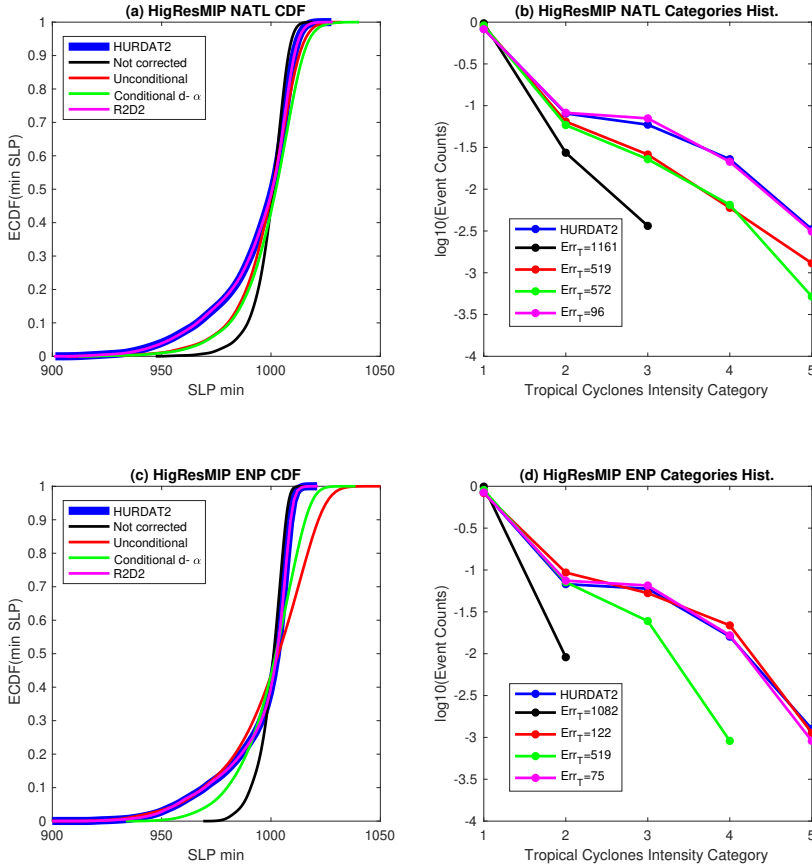


**Fig. 10** Unconditional, R2D2, and conditional dynamical systems metrics bias corrections for the IPSL-CM6A-ATM-ICO-HR model. The conditional dynamical systems metrics bias corrections uses the best  $d_c = 19$  and  $\alpha_c = 0.165$  parameters combination from ERA5 cg. Panels (a,c) show Empirical Cumulative Density Functions (ECDFs) and (b,d) histograms of category intensities for the North Atlantic [NATL] (a,b) and eastern North Pacific [ENP] (c,d) basins.

510 energy  $uv$  and potential vorticity  $PV$  at 850 hPa. We have observed that the  
 511 dynamical systems metrics are able to track intense cyclones as organized  
 512 states of the dynamics, yielding low dimensionality and high coupling. While  
 513 all bias corrections improve the bulk statistics of tropical cyclone intensity  
 514 representation in our datasets, the categorisation for individual cyclones is  
 515 not always improved. The conditional bias correction tends to perform better  
 516 when the underlying relationship between the predictors and the response  
 517 variable is strong and well-defined, whereas the unconditional bias correction  
 518 can be more effective when the relationship is weaker or more variable. For  
 519 the HighResMIP model, the best bias correction is the multivariate R2D2  
 520 correction which takes into account the relationships among SLP,  $d$  and  $\alpha$ . This  
 521 suggests that accounting for the multivariate dependence structures associated

with the dynamical systems metrics is crucial to correcting the distribution of tropical cyclone intensities. We also observe non-negligible differences in the bias correction performances in the two Atlantic and Pacific basins that could be further investigated in the future. For example, the conditional bias correction in the HighResMIP model underperforms in the ENP relative to its unconditional counterpart, yet this is not observed in the reanalysis. We also point out that while the optimal combination of  $d$  and  $\alpha$  shows some variability when reshuffling the data, the changes are small. While it is true that the sample used in this study is large, with over 10000 storm timesteps, we would need to repeat the grid-search if significant changes in the storm sample occur, such as a major shift in the frequency or intensity of storms.

These considerations have a number of concrete implications for current research on tropical cyclones. Current GCMs — and even reanalysis products — struggle in reproducing minimum sea-level pressures comparable to those observed. Our study offers a way of mapping intense cyclones in  $d, \alpha$  space and a procedure to correct biases in both century-long reanalysis products and high-resolution GCMs. This, in turn, may provide a strategy for studying changes in tropical cyclone intensity driven by anthropogenic forcing. Indeed, while  $d$  and  $\alpha$  may not be used to provide a deterministic indication of cyclone intensity, they do provide a robust constraint for statistical correction. The large range of local dimensions associated with the dynamics of different phases of tropical cyclones may explain why it is so difficult to adequately represent them in numerical models. Follow-up studies will include the use of a larger set of HighResMIP data under different forcing scenarios, to test systematically the R2D2 correction on model data. The bias correction procedures will then be adapted to take into account the non-stationarities introduced by anthropogenic forcing, e.g. by replacing the quantile-quantile mapping with a CDF-t correction (Vrac et al, 2012) allowing to account for climate change in the correction procedure. A further avenue for future work will be to move from the pointwise correction of minimum SLP performed here, to correcting the spatial structure of the field, using multivariate bias correction techniques (e.g. Cannon, 2018; Vrac, 2018; Robin et al, 2019; Vrac and Thao, 2020) or tools from machine learning (e.g. François et al, 2021).

## Statements and declarations

- Funding: the authors acknowledge the support of the INSU-CNRS-LEFE-MANU grant (project CROIRE), as well as the grant ANR-19-ERC7-0003 (BOREAS). This work has received support from the European Union’s Horizon 2020 research and innovation programme (Grant agreement No. 101003469, XAIDA) and from the European Research Council (ERC) under the European Union’s Horizon 2020 research and innovation programme (Grant agreement No. 948309, CENÆ project). MV was partly supported by the “COESION” project funded by the French National program LEFE

(Les Enveloppes Fluides et l'Environnement), as well as the French National "Explore2" project funded by the French Ministry of Ecological Transition (MTE) and the French Office for Biodiversity (OFB).

- 568 • Conflict of interest: The authors declare no conflict of interest.
- 569 • Ethics approval: Not applicable.
- 570 • Consent to participate: Not applicable.
- 571 • Consent for publication: Not applicable.
- 572 • Availability of data and materials: ERA5 is the latest climate reanalysis being produced by ECMWF as part of implementing the EU-funded Copernicus Climate Change Service (C3S), providing hourly data on atmospheric, land-surface and sea-state parameters together with estimates of uncertainty from 1979 to present day. ERA5 data are available on the C3S Climate Data Store on regular latitude-longitude grids at 0.25° x 0.25° resolution at <https://cds.climate.copernicus.eu>, accessed on 2022-04-11. The Atlantic hurricane database (HURDAT2) 1851-2020 is publicly available at <https://www.nhc.noaa.gov/data/hurdat/hurdat2-1851-2020-020922.txt>, accessed on 2022-04-11. The IPSL simulations are available upon request.
- 582 • Code availability: The main results of this work were obtained using Matlab. The scripts for computing the dimension and the corecurrence coefficient are available by downloading the package <https://fr.mathworks.com/matlabcentral/fileexchange/95768-attractor-local-dimension-and-local-persistence-computation>
- 587 • Authors' contributions: DF performed the analysis. DF and GM co-designed the analyses. ST and SB prepared the datasets. All authors participated to the manuscript preparation and contributed to the interpretation of the results.

## 591 References

- 592 Bhalachandran S, Chavas DR, Jr FDM, et al (2020) Characterizing the  
593 Energetics of Vortex-Scale and Sub-Vortex-Scale Asymmetries during Tropi-  
594 cal Cyclone Rapid Intensity Changes. *Journal of the Atmospheric Sci-*  
595 *ences* 77(1):315–336. <https://doi.org/10.1175/JAS-D-19-0067.1>, URL <https://journals.ametsoc.org/view/journals/atsc/77/1/jas-d-19-0067.1.xml>, pub-  
596 lisher: American Meteorological Society Section: *Journal of the Atmospheric*  
597 *Sciences*
- 599 Boucher O, Servonnat J, Albright AL, et al (2020) Presentation and evaluation  
600 of the ipsl-cm6a-lr climate model. *Journal of Advances in Modeling Earth*  
601 *Systems* 12(7):e2019MS002,010
- 602 Brunetti M, Kasparian J, V erard C (2019) Co-existing climate attractors in a  
603 coupled aquaplanet. *Climate Dynamics* 53(9-10):6293–6308
- 604 Camargo SJ, Wing AA (2016) Tropical cyclones in climate models. *WIREs*  
605 *Clim Change* 7:211–237. <https://doi.org/https://doi.org/10.1002/wcc.373>

*Correcting biases in tropical cyclone intensities in low-resolution datasets using dynamical s*

- 606 Camargo SJ, Emanuel KA, Sobel AH (2007) Use of a genesis potential index  
607 to diagnose ENSO effects on tropical cyclone genesis. *Journal of Climate*  
608 20(19):4819–4834
- 609 Cannon AJ (2018) Multivariate quantile mapping bias correction: an n-  
610 dimensional probability density function transform for climate model  
611 simulations of multiple variables. *Climate dynamics* 50(1):31–49
- 612 Cannon AJ, Sobie SR, Murdock TQ (2015) Bias correction of gcm precipitation  
613 by quantile mapping: how well do methods preserve changes in quantiles  
614 and extremes? *Journal of Climate* 28(17):6938–6959
- 615 Cao L (1997) Practical method for determining the minimum embedding  
616 dimension of a scalar time series. *Physica D: Nonlinear Phenomena* 110(1-  
617 2):43–50
- 618 Caron LP, Jones CG, Winger K (2011) Impact of resolution and downscal-  
619 ing technique in simulating recent atlantic tropical cyclone activity. *Climate*  
620 *dynamics* 37(5):869–892
- 621 Carstens JD, Wing AA (2020) Tropical cyclogenesis from self-aggregated  
622 convection in numerical simulations of rotating radiative-convective  
623 equilibrium. *Journal of Advances in Modeling Earth Systems*  
624 12(5):e2019MS002,020
- 625 Chang EK, Guo Y (2007) Is the number of north atlantic tropical cyclones sig-  
626 nificantly underestimated prior to the availability of satellite observations?  
627 *Geophysical Research Letters* 34(14)
- 628 Crisanti A, Falcioni M, Vulpiani A, et al (1991) Lagrangian chaos: transport,  
629 mixing and diffusion in fluids. *La Rivista del Nuovo Cimento* (1978-1999)  
630 14(12):1–80
- 631 De Luca P, Messori G, Pons FM, et al (2020) Dynamical systems theory  
632 sheds new light on compound climate extremes in europe and eastern  
633 north america. *Quarterly Journal of the Royal Meteorological Society*  
634 146(729):1636–1650
- 635 Dubos T, Dubey S, Tort M, et al (2015) Dynamico-1.0, an icosahedral hydro-  
636 static dynamical core designed for consistency and versatility. *Geoscientific*  
637 *Model Development* 8(10):3131–3150
- 638 Dunkerton TJ, Montgomery M, Wang Z (2009) Tropical cyclogenesis in a  
639 tropical wave critical layer: Easterly waves. *Atmospheric Chemistry and*  
640 *Physics* 9(15):5587–5646



- 641 Emanuel K (2021) Response of global tropical cyclone activity to increasing  
642 CO<sub>2</sub>: Results from downscaling CMIP6 models. *J Climate* 34:57–70. <https://doi.org/10.1175/JCLI-D-20-0367.1>  
643
- 644 Emanuel KA (1986) An air-sea interaction theory for tropical cyclones. part i:  
645 Steady-state maintenance. *Journal of Atmospheric Sciences* 43(6):585–605
- 646 Emanuel KA (1997) Some aspects of hurricane inner-core dynamics and ener-  
647 getics. *Journal of the Atmospheric Sciences* 54:1014–1026. [https://doi.org/](https://doi.org/10.1175/1520-0469(1997)054<1014:SAOHIC>2.0.CO;2)  
648 [10.1175/1520-0469\(1997\)054<1014:SAOHIC>2.0.CO;2](https://doi.org/10.1175/1520-0469(1997)054<1014:SAOHIC>2.0.CO;2)
- 649 Faranda D, Messori G, Yiou P (2017) Dynamical proxies of north atlantic  
650 predictability and extremes. *Scientific reports* 7:41,278
- 651 Faranda D, Lembo V, Iyer M, et al (2018) Computation and characterization  
652 of local subfilter-scale energy transfers in atmospheric flows. *Journal of the*  
653 *Atmospheric Sciences* 75(7):2175–2186
- 654 Faranda D, Alvarez-Castro MC, Messori G, et al (2019) The hammam effect or  
655 how a warm ocean enhances large scale atmospheric predictability. *Nature*  
656 *communications* 10(1):1–7
- 657 Faranda D, Messori G, Yiou P (2020) Diagnosing concurrent drivers of weather  
658 extremes: application to warm and cold days in north america. *Climate*  
659 *Dynamics* 54(3):2187–2201
- 660 Faranda D, Messori G, Yiou P, et al (2023) Dynamical footprints of hurricanes  
661 in the tropical dynamics. *Chaos: An Interdisciplinary Journal of Nonlinear*  
662 *Science* 33(1):013,101
- 663 François B, Thao S, Vrac M (2021) Adjusting spatial dependence of cli-  
664 mate model outputs with cycle-consistent adversarial networks. *Climate*  
665 *Dynamics* 57(11):3323–3353
- 666 Freitas ACM, Freitas JM, Todd M (2010) Hitting time statistics and extreme  
667 value theory. *Probability Theory and Related Fields* 147(3-4):675–710
- 668 Fu B, Peng MS, Li T, et al (2012) Developing versus nondeveloping distur-  
669 bances for tropical cyclone formation. part ii: Western north pacific. *Monthly*  
670 *weather review* 140(4):1067–1080
- 671 Grinsted A, Ditlevsen P, Christensen JH (2019) Normalized us hurricane dam-  
672 age estimates using area of total destruction, 1900- 2018. *Proceedings of the*  
673 *National Academy of Sciences* 116(48):23,942–23,946
- 674 Gualandi A, Avouac JP, Michel S, et al (2020) The predictable chaos of slow  
675 earthquakes. *Science advances* 6(27):eaaz5548

*Correcting biases in tropical cyclone intensities in low-resolution datasets using dynamical s*

- 676 Haarsma RJ, Roberts MJ, Vidale PL, et al (2016) High resolution model inter-  
677 comparison project (HighResMIP v1. 0) for CMIP6. Geoscientific Model  
678 Development 9(11):4185–4208
- 679 Hersbach H, Bell B, Berrisford P, et al (2020) The era5 global reanalysis.  
680 Quarterly Journal of the Royal Meteorological Society 146(730):1999–2049
- 681 Hochman A, Alpert P, Harpaz T, et al (2019) A new dynamical systems  
682 perspective on atmospheric predictability: Eastern mediterranean weather  
683 regimes as a case study. Science advances 5(6):eaau0936
- 684 Hochman A, Messori G, Quinting JF, et al (2021a) Do atlantic-  
685 european weather regimes physically exist? Geophysical Research Letters  
686 48(20):e2021GL095,574
- 687 Hochman A, Scher S, Quinting J, et al (2021b) A new view of heat wave  
688 dynamics and predictability over the eastern mediterranean. Earth System  
689 Dynamics 12(1):133–149
- 690 Hourdin F, Rio C, Grandpeix JY, et al (2020) Lmdz6a: The atmospheric com-  
691 ponent of the ipsl climate model with improved and better tuned physics.  
692 Journal of Advances in Modeling Earth Systems 12(7):e2019MS001,892
- 693 Kim D, Moon Y, Camargo SJ, et al (2018) Process-oriented diagnosis of trop-  
694 ical cyclones in high-resolution gcms. Journal of Climate 31(5):1685–1702
- 695 Klotzbach PJ, Bell MM, Bowen SG, et al (2020) Surface pressure a more  
696 skillful predictor of normalized hurricane damage than maximum sustained  
697 wind. Bulletin of the American Meteorological Society 101(6):E830–E846
- 698 Knaff JA, Sampson CR, Kucas ME, et al (2021) Estimating tropical cyclone  
699 surface winds: Current status, emerging technologies, historical evolution,  
700 and a look to the future. Tropical Cyclone Research and Review 10:125–150.  
701 <https://doi.org/https://doi.org/10.1016/j.tcr.2021.09.002>
- 702 Knutson T, Camargo SJ, Chan JCL, et al (2019) Tropical cyclones and climate  
703 change assessment: Part I: Detection and Attribution. Bull Amer Meteor  
704 Soc 100:1987–2007. <https://doi.org/10.1175/BAMS-D-18-0189.1>
- 705 Knutson T, Camargo SJ, Chan JC, et al (2020) Tropical cyclones and climate  
706 change assessment: Part ii: Projected response to anthropogenic warming.  
707 Bulletin of the American Meteorological Society 101(3):E303–E322
- 708 Krishnamurti T, Pattnaik S, Stefanova L, et al (2005) The hurricane intensity  
709 issue. Monthly weather review 133(7):1886–1912

- 710 Landsea CW, Franklin JL (2013) Atlantic hurricane database uncertainty  
711 and presentation of a new database format. *Monthly Weather Review*  
712 141(10):3576–3592
- 713 Lee CY, Camargo SJ, Sobel AH, et al (2020) Statistical–dynamical down-  
714 scaling projections of tropical cyclone activity in a warming climate: Two  
715 diverging genesis scenarios. *J Climate* 33:4815–4834. [https://doi.org/10.](https://doi.org/10.1175/JCLI-D-19-0452.1)  
716 [1175/JCLI-D-19-0452.1](https://doi.org/10.1175/JCLI-D-19-0452.1)
- 717 Levich E, Tzvetkov E (1985) Helical inverse cascade in three-dimensional tur-  
718 bulence as a fundamental dominant mechanism in mesoscale atmospheric  
719 phenomena. *Physics reports* 128(1):1–37
- 720 Li H, Sheffield J, Wood EF (2010) Bias correction of monthly precipitation and  
721 temperature fields from intergovernmental panel on climate change ar4 mod-  
722 els using equidistant quantile matching. *Journal of Geophysical Research:*  
723 *Atmospheres* 115(D10)
- 724 Lorenz EN (1990) Can chaos and intransitivity lead to interannual variability?  
725 *Tellus A* 42(3):378–389
- 726 Lucarini V, Faranda D, Wouters J (2012) Universal behaviour of extreme value  
727 statistics for selected observables of dynamical systems. *Journal of statistical*  
728 *physics* 147(1):63–73
- 729 Lucarini V, Faranda D, de Freitas JMM, et al (2016) *Extremes and recurrence*  
730 *in dynamical systems*. John Wiley & Sons
- 731 Manganello JV, Hodges KI, Kinter III JL, et al (2012) Tropical cyclone clima-  
732 tology in a 10-km global atmospheric gcm: toward weather-resolving climate  
733 modeling. *Journal of Climate* 25(11):3867–3893
- 734 Maraun D (2016) Bias correcting climate change simulations—a critical review.  
735 *Current Climate Change Reports* 2(4):211–220
- 736 Maraun D, Widmann M (2018) Cross-validation of bias-corrected cli-  
737 mate simulations is misleading. *Hydrology and Earth System Sciences*  
738 22(9):4867–4873. <https://doi.org/10.5194/hess-22-4867-2018>, URL [https://](https://hess.copernicus.org/articles/22/4867/2018/)  
739 [hess.copernicus.org/articles/22/4867/2018/](https://hess.copernicus.org/articles/22/4867/2018/)
- 740 Messori G, Faranda D (2021) Characterising and comparing different palaeo-  
741 climates with dynamical systems theory. *Climate of the Past* 17(1):545–563
- 742 Messori G, Caballero R, Faranda D (2017) A dynamical systems approach  
743 to studying midlatitude weather extremes. *Geophysical Research Letters*  
744 44(7):3346–3354

*Correcting biases in tropical cyclone intensities in low-resolution datasets using dynamical s*

- 745 Messori G, Harnik N, Madonna E, et al (2021) A dynamical systems character-  
746 ization of atmospheric jet regimes. *Earth System Dynamics* 12(1):233–251
- 747 Michelangeli PA, Vrac M, Loukos H (2009) Probabilistic downscaling  
748 approaches: Application to wind cumulative distribution functions. *Geo-*  
749 *physical Research Letters* 36(11)
- 750 Montgomery MT, Smith RK (2017) Recent developments in the fluid dynamics  
751 of tropical cyclones. *Annual Review of Fluid Mechanics* 49:541–574
- 752 Moon Y, Kim D, Camargo SJ, et al (2020) Azimuthally averaged wind and  
753 thermodynamic structures of tropical cyclones in global climate models and  
754 their sensitivity to horizontal resolution. *J Climate* 33:1575 – 1595. <https://doi.org/10.1175/JCLI-D-19-0172.1>  
755
- 756 Muller CJ, Roms DM (2018) Acceleration of tropical cyclogenesis by self-  
757 aggregation feedbacks. *Proceedings of the National Academy of Sciences*  
758 115(12):2930–2935
- 759 Murakami H, Wang Y, Yoshimura H, et al (2012) Future changes in tropical  
760 cyclone activity projected by the new high-resolution mri-agcm. *Journal of*  
761 *Climate* 25(9):3237–3260
- 762 Peng MS, Fu B, Li T, et al (2012) Developing versus nondeveloping dis-  
763 turbances for tropical cyclone formation. part i: North atlantic. *Monthly*  
764 *weather review* 140(4):1047–1066
- 765 Roberts MJ, Camp J, Seddon J, et al (2020a) Impact of model resolution  
766 on tropical cyclone simulation using the highresmip–primavera multimodel  
767 ensemble. *Journal of Climate* 33(7):2557–2583
- 768 Roberts MJ, Camp J, Seddon J, et al (2020b) Projected future changes  
769 in tropical cyclones using the CMIP6 HighResMIP multimodel ensemble.  
770 *Geophysical Research Letters* 47(14):e2020GL088,662
- 771 Robin Y, Vrac M, Naveau P, et al (2019) Multivariate stochastic bias cor-  
772 rections with optimal transport. *Hydrology and Earth System Sciences*  
773 23(2):773–786
- 774 Rotunno R, Chen Y, Wang W, et al (2009) Large-eddy simulation of an ideal-  
775 ized tropical cyclone. *Bull Amer Meteor Soc* 90:1783–1788. [https://doi.org/](https://doi.org/10.1175/2009BAMS2884.1)  
776 [10.1175/2009BAMS2884.1](https://doi.org/10.1175/2009BAMS2884.1)
- 777 Schubert S, Lucarini V (2015) Covariant lyapunov vectors of a quasi-  
778 geostrophic baroclinic model: analysis of instabilities and feedbacks. *Quar-*  
779 *terly Journal of the Royal Meteorological Society* 141(693):3040–3055

- 780 Simpson RH, Saffir H (1974) The hurricane disaster potential scale. *Weather-*  
781 *wise* 27(8):169
- 782 Smith AB, Katz RW (2013) Us billion-dollar weather and climate disasters:  
783 data sources, trends, accuracy and biases. *Natural hazards* 67(2):387–410
- 784 Sugi M, Murakami H, Yoshida K (2017) Projection of future changes in the  
785 frequency of intense tropical cyclones. *Climate Dynamics* 49:619–632
- 786 Tang J, Byrne D, Zhang JA, et al (2015) Horizontal transition of turbu-  
787 lent cascade in the near-surface layer of tropical cyclones. *Journal of the*  
788 *Atmospheric Sciences* 72(12):4915–4925
- 789 Ullrich PA, Zarzycki CM, McClenny EE, et al (2021) Tempestextremes v2. 1:  
790 a community framework for feature detection, tracking and analysis in large  
791 datasets. *Geoscientific Model Development Discussions* pp 1–37
- 792 Vrac M (2018) Multivariate bias adjustment of high-dimensional climate sim-  
793 ulations: the rank resampling for distributions and dependences (r 2 d 2)  
794 bias correction. *Hydrology and Earth System Sciences* 22(6):3175–3196
- 795 Vrac M, Thao S (2020) R 2 d 2 v2. 0: accounting for temporal dependences  
796 in multivariate bias correction via analogue rank resampling. *Geoscientific*  
797 *Model Development* 13(11):5367–5387
- 798 Vrac M, Drobinski P, Merlo A, et al (2012) Dynamical and statistical down-  
799 scaling of the french mediterranean climate: uncertainty assessment. *Natural*  
800 *Hazards and Earth System Sciences* 12(9):2769–2784
- 801 Vulpiani A (2010) *Chaos: from simple models to complex systems*, vol 17.  
802 World Scientific
- 803 Wolf A, Swift JB, Swinney HL, et al (1985) Determining lyapunov exponents  
804 from a time series. *Physica D: Nonlinear Phenomena* 16(3):285–317
- 805 Yoshida K, Sugi M, Mizuta R, et al (2017) Future changes in tropical cyclone  
806 activity in high-resolution large-ensemble simulations. *Geophysical Research*  
807 *Letters* 44(19):9910–9917
- 808 Zhao M, Held IM (2010) An analysis of the effect of global warming on  
809 the intensity of atlantic hurricanes using a gcm with statistical refinement.  
810 *Journal of Climate* 23(23):6382–6393